EUROPEAN ORGANIZATION FOR NUCLEAR RESEARCH

CERN-PPE/93-20
January 13, 1993

Test Results of an Electromagnetic Calorimeter with 0.5 mm Scintillating Fibers Readout

The RD1 Collaboration

J. Badier[1)], N. Bouhemaid[2)], S. Buontempo[3)], P. Busson[1)], L. Calôba[4)], P. Cattaneo[5)], C. Charlot[1)], A. Chekhtman[6)], M-C. Cousinou[6)], S. Dagoret[7)], A. Dell'Acqua[5)], A. Ereditato[3)], R. Ferrari[5)], D. Fouchez[6)], L. Fredj[2)], G. Fumagalli[5)], J-M. Gaillard[8,11)], G. Goggi[5)], A. Gomes[9)], T. Hansl-Kozanecka[7)], A. Henriques[8,9)], F. Kovacs[7)], L. Linssen[8)], M. Livan[5)], J. Lory[7)], A. Maio[9,12)], B. Michel[2)], G. Montarou[2)], R. Nacasch[6)], E. Nagy[6)], H.P. Paar[10)], D. Pallin[2)], E. Pennacchio[5)], L. Peralta[9)], L. Poggioli[8)], G. Polesello[5)], F. Riccardi[3)], A. Rimoldi[5)], J.M. Seixas[4,8)], M. Sivertz[10)], M.N. Souza[4)], Z.D. Thomé[4)], S. Tisserant[6)], B. Tomé[9)], F. Vazeille[2)], V. Vercesi[5)], R. Wigmans[13)], R. Zitoun[7)]

1) *LPNHE, Ecole Polytechnique, Palaiseau, France*
2) *LPPCF, Université Blaise Pascal, Clermont-Ferrand, France*
3) *Università di Napoli and INFN Sez. Napoli, Italy*
4) *COPPE/EE/UFRJ, Rio de Janeiro, Brazil*
5) *Università di Pavia and INFN Sez. Pavia, Italy*
6) *CPPM, Marseille, France*
7) *LPNHE, Université Paris VI&VII, Paris, France*
8) *CERN, Geneva, Switzerland*

9) *LIP, Lisbon, Portugal*

10) *University of California, San Diego, USA*

11) *LAL, Orsay, France*

12) *CFNUL, Lisbon, Portugal*

13) *Texas Tech University, Lubbock, USA*

Abstract

We report on an experimental study of the performance of an electromagnetic calorimeter consisting of thin (0.5 mm diameter) scintillating plastic fibers embedded in lead. Because of the small sampling fraction (3.5% for minimum ionizing particles), this detector is quite compact, with an effective radiation length of 7.2 mm and a Molière radius of 20 mm. Because of the very frequent shower sampling provided by the fibers, the energy resolution is nevertheless good : $9.2\%/\sqrt{E(GeV)}$ for electromagnetic (e.m.) showers, with a small, angle dependent constant term. A non-uniformity in the response is observed at the 2 % level across the calorimeter. In spite of the small sampling fraction the light yield is not a limiting factor in this calorimeter: we measured $\sim$ 500 photoelectrons per GeV shower energy. The position resolution for electrons and two e.m. showers separation have been studied. The fibers sticking out of the back of the detector do not appear to affect the measurements of hadronic showers.

(Submitted to Nuclear Instruments and Methods in Physics Research)

1. INTRODUCTION

The use of scintillating fibers as active material in calorimeters has a number of attractive features in term of speed, ease of read-out and hermiticity of the detector. Scintillating fibers deliver fast signals[1-3] at very low noise level[4,5] , allow for a compact detector, can operate in Mrad/yr radiation environments[6,7] and can lead to a cheap detector design. In addition the calorimeter can be made compensating by an appropriate choice of the absorber and the sampling fraction[8,9] . Because of these reasons, scintillating-fiber calorimeters are considered an attractive option for experiments at the future multi-TeV proton-proton colliders LHC and SSC[10,11,12] .

The basic calorimetric properties for electron, hadron, jet and muon detection of this type of calorimeter were extensively studied by Acosta *et al.*[2,9,13,14] . The energy resolution was measured to be $12.9\%/\sqrt{E} + 1.2\%$, with E in GeV, for electron induced showers and $30.6\%/\sqrt{E} + 1.0\%$ for pions[9] , for a detector made of 1.0 mm thick plastic fibers embedded in lead with a volume ratio of 4:1, which corresponds to a sampling fraction of $\sim 2.5\%$ for showers (3.5% for minimum ionizing particles -mip-)[14] . These resolutions are not considered suitable in view of the physics goals of LHC/SSC experiments which are being contemplated[10,11,12] and which, in particular, require better e.m. energy resolution and uniformity, possibly at the expense of the hadronic performance.

The energy resolution of a sampling calorimeter is among other factors determined by the sampling fraction, i.e. the fraction of the shower energy deposited in the active calorimeter medium. This fraction was very small for the detectors built by Acosta *et al.*, because of the compensation requirement. If this fraction is increased, considerably better energy resolutions can be achieved. This was experimentally demonstrated by the JETSET Collaboration[15] , who reported an e.m. energy resolution of $6.5\%/\sqrt{E}$ for a fiber calorimeter with a sampling fraction of $\sim 17\%$ (for mip's). Burmeister *et al.*[16] measured a resolution of $\sim 8\%/\sqrt{E}$ for a calorimeter containing fiber ribbons, and which had a sampling fraction of $\sim 18\%$ (for mip's).

However, such a large increase of the sampling fraction has several disadvantages. Apart from the already mentioned departure from the compensation condition, the detector also becomes less compact : because of the increased fraction of low-density material, shower dimensions increase, requiring a larger instrument to contain them and longer distances between particles to recognize the produced showers as separated.

Another way of improving the energy resolution of this type of calorimeter which is not subject to the mentioned disadvantages consists of making the sampling more frequent by using thinner fibers. This is the approach that was chosen in this study. The lead to plastic ratio was the same as for the detector from ref. 9, but fibers with a diameter of 0.5 mm instead of 1.0 mm were used. Therefore, a given detector volume contains four times as many sampling elements (fibers) as the detector of Acosta *et al.*,

while the sampling fractions are approximately the same. The e.m. shower detection with this detector was studied in great detail using high-energy electron beams. Since the very fine sampling provided by this calorimeter is only intended for the detection of e.m. showers, the detector was not made deeper than needed for the containment of such showers. In a realistic application, this device could be used as the e.m. section of a calorimeter of which the hadronic section has the same composition (lead:plastic ratio), but with a much more crude sampling frequency (e.g. thicker fibers). In order to test the feasibility of this idea, some measurements on pions were done as well.

In section 2, the detector, its construction and calibration and the experimental set-up are described. Details on the analysis of the experimental data are given in section 3. The experimental results are presented in section 4. Section 5 contains a summary and conclusions.

2. EXPERIMENTAL SET-UP

2.1 The calorimeter

The measurements were performed with a calorimeter consisting of lead and scintillating plastic fibers* . The latter have a diameter of 0.5 mm and a length of 50 cm. The detector was assembled out of thick lead sheets ($0.1 \times 8 \times 30$ cm^3), in which U-shaped grooves were machined (fig. 1a), the fibers being inserted in the grooves. The plates are stacked together to form a structure with a front surface of 8×8 cm^2 and a depth of 30 cm. This structure is held mechanically, no glue or solder is applied (the total weight amounts to less than 20 kg).

The detector contains in total 5472 fibers. The volume ratio lead to plastic is approximately 4:1, chosen as such to make the calorimeter (approximately) compensating[9] All fibers run parallel to one another in the direction of the incoming particles.

The calorimeter is subdivided in four square towers with a surface of 4×4 cm^2 each (fig. 1b). This is achieved by grouping the fibers sticking out at the rear end of the detector. The fibers were bunched together into hexagonal structures, machined and diamond cut, and coupled through light guides to photomultipliers (PM)** , equipped with yellow filters*** . Before inserting the fibers, their upstream ends were diamond cut and made reflective by aluminium sputtering, such as to make the response more uniform as a function of the position along the fiber[18] .

The large lead fraction ($\sim$ 78% of the volume) makes this calorimeter very compact. The radiation length (X_0) amounts to 7.2 mm, the Molière radius (R_M) 20 mm, the

* 3HF(200 ppm) + PTP, polystyrene base, Kuraray Company
** Philips XP 2961, diameter 1", 8-stage, green extended photocathode
*** Kodak Wratten #3

nuclear interaction length (λ_I) 21.0 cm[17] and the effective density 9.0 g/cm^3. The depth of the calorimeter corresponds therefore to 41 X_0, and laterally it measures about 4 R_M across.

To increase the dynamic range of the read-out, the anode signal from each PM was fed into an active splitter, one output of which was sent unchanged into a 12-bit charge ADC, the other output was amplified by a factor $\sim$ 10 before being fed into an ADC. The gain in the PM tubes was set to $\sim$ 4 pC/GeV, the ADC response being 4 counts/pC. The data discussed in this paper were taken with an ADC gate width of 400 ns. Sparse data readout was enabled: signals smaller than 4 counts above the pedestal value were not recorded. This corresponds to a cutoff of 25 MeV in the amplified channels.

2.2 The beam line

The measurements were performed in the H2 beam line of the SPS at CERN. The calorimeter was mounted on a platform that could move horizontally and vertically with respect to the beam line, with a precision of about 0.1 mm. The detector was rotated by 45 degrees around the beam line as shown in fig. 1b. The detector could also be rotated around its vertical axis, so that the particles could be sent into the detector at a chosen angle θ_z (usually a few degrees) with respect to the fiber axis, in the horizontal plane.

Further upstream of the calorimeter, a trigger counter telescope was installed. It consists of 5 scintillation counters (S1 - S5) and 2 drift chambers with x,y readout (BC1, BC2), the distance between the 2 chambers being 1.8 m. The layout is shown in fig. 2.

Electron beams of 10, 20, 40, 80 and 150 GeV were sent into the detector at a small angle θ_z with respect to the fiber axis. The beam rates were $10^2 - 10^3$ particles per 2.6 s long spills, repeated every 14 s. At high energies ($\geq$ 40 GeV) the beams were very clean, the contamination of pions being below the 1% level.

2.3 Calibration of the calorimeter

The calorimeter was calibrated with a 40 GeV electron beam. About 2000 electrons were sent into the central region of each of the four individual towers, at an angle θ_z of 2^0 with respect to the fiber axis. In this way, on average $\sim$ 92% of the shower energy was deposited in the tower concerned. Off-line, the calibration constants (the relation between picocoulombs and GeV's for each individual tower) could be determined with a statistical precision of $\sim$ 0.3% from this data. The PM bases were cooled under continuous nitrogen flow to provide a stable response. Moreover, the PM were recalibrated every 6 hours to remove any temperature effect on the response. Because of systematic effects, due to fluctuations in the fiber-to-fiber response and in the local sampling frac-

tion, etc. the tower-to-tower calibration is less precisely known. We will come back to this point in sect. 4.3.

3. EXPERIMENTAL DATA AND METHODS

The results described in the following sections were obtained by analyzing the following sets of data:

- Electrons of 10, 20, 40, 80 and 150 GeV entering the fiber calorimeter in the central region at an angle $\theta_z = 2^0$. Typically, $\sim$ 3000 events were accumulated per run.
- Angular scans with 40 GeV electrons entering the central region of the calorimeter at the following angles θ_z: -2, -1, -0.5, 0, 0.2, 0.5, 1.0, 1.5, 2.0, 2.5, 3.0, 4.0 degrees (overall accuracy 0.2^0). Also in this case, $\sim$ 3000 events were accumulated per run.
- A scan with 40 GeV electrons at $\theta_z = 90^0$, the so-called z-scan, intended to measure the attenuation length of the fibers in the calorimeter. The beam was moved in steps of 5 cm from the front face to the rear end of the calorimeter. 3000 events were collected for each run.
- A grid scan, in which 40 GeV electrons were sent into the calorimeter at 36 different impact points, located on a square grid with a period of 1 cm, covering an area of 6×6 cm^2 in a rather uniform way with entries. In total, 10^5 events were accumulated.
- Pions of 20 and 150 GeV entering the calorimeter in the meeting point of 4 cells or in the center of 1 cell, for $\theta_z = 0^0, 2^0$ and $180^0, 182^0$. In the latter case, the particles traversed the readout section of the calorimeter (PM's, fiber bunches) before entering the lead volume. Typically, $\sim$ 5000 events were accumulated per run.
- Dedicated runs with neutral density filters.

Off-line event selection required a single track, by cutting on the pulse height of the scintillation counters S1, S2 and S3 between 0.5 and 1.7 times the mip value. Particles travelling at anomalous angles were removed by requiring that the x and y coordinates measured in the two beam chambers agree within 1 cm. Beam halo particles were removed by cuts on x and y in the beam chambers.

4. EXPERIMENTAL RESULTS

4.1 The energy resolution and its angular dependence

The energy resolution for electrons was studied with particles of 10, 20, 40, 80 and 150 GeV entering the calorimeter at different angles θ_z in the horizontal plane. The signal distributions are very well described by Gaussian functions, except at very small angle θ_z ($< 1^0$), as shown in fig. 3. The energy resolution and the average signal were determined from Gaussian fits without any constraint. The results are listed in the second and third columns of table 1, for $\theta_z = 2^0$, at which angle most of the measurements were performed.

The energy resolution for $\theta_z = 2^0$ is plotted as a function of the energy in fig. 4. The energy scale is linear in $1/\sqrt{E}$. It is clear that, apart from a term scaling as $1/\sqrt{E}$, there is an energy independent contribution to the energy resolution. We tried two fits, of which the results are also shown in the figure, to account for this effect. The results are the following :

$$\frac{\sigma}{E} = \frac{(9.2 \pm 0.3)\%}{\sqrt{E}} + (0.63 \pm 0.05)\% \qquad (\chi^2 = 2.6/\text{d.o.f.}) \qquad (1a)$$

$$\frac{\sigma}{E} = \frac{(10.9 \pm 0.2)\%}{\sqrt{E}} \oplus (1.11 \pm 0.05)\% \qquad (\chi^2 = 3.2/\text{d.o.f.}) \qquad (1b)$$

with E in GeV. As observed before[9] , the linear fit (1a) gives a somewhat better description of the experimental data than the quadratic one. Similar data were obtained for other values of the angle θ_z. For each individual angle, at E = 40 GeV, fits of the type (1a) were performed:

$$\sigma/E(\theta_z) = a/\sqrt{E} + b(\theta_z) \qquad (1c)$$

assuming a constant value for the sampling term, which was found in previous studies to be almost independent of θ_z[18] . The dependence of b as a function of θ_z is shown in fig. 5. When these results are compared with the ones published by Acosta *et al.*[9] for a similar detector with 1 mm thick fibers and the same sampling fraction, it turns out that the scaling term of our detector has improved by a factor approximately $\sqrt{2}$ and the constant term by about a factor 2. This is in agreement with simple models which predict a scaling as the ratio of the square-roots of the fiber diameters, and b as the square-root of the number of fibers involved in the shower development[19] .

4.2 The signal linearity

The average calorimeter response is shown as a function of the electron energy in fig. 6 (full circles), for the $\theta_z = 2^0$ data. The signal per unit energy is almost constant as a function of energy. The response is somewhat too high only at the highest energies. This might be due to the effect of light attenuation in the fibers. At higher energy, in

fact, the scintillation light is on average produced deeper inside the calorimeter and, therefore, it is less attenuated on its way to the PM's.

In order to estimate this effect quantitatively, we analyzed the data taken at $\theta_z = 90^0$ (the z-scan data). The showers are not fully contained in the detector when it is exposed this way, but since the containment is always the same, the average signals give a very good indication of the light attenuation in the fibers. Figure 7 shows the average signal as a function of the distance over which the light has to travel to reach the PM's. When these data are fitted to a single exponential, the attenuation length is found to be ~ 1.5 m. The center of gravity of the light production shifts logarithmically to greater depth as the energy increases[20] . At 150 GeV, it is shifted by $\sim 2.6\ X_0$ ($= 2.2$ cm) compared to 10 GeV, which should therefore produce a 1.5% increase in the response. We correct for this effect by taking into account the shift of the center of gravity (open circles in 6). We also include uncertainties on the beam energy value, due to hysteresis effects at low energy (represented by the 2 hyperbolae in 6). The resulting response exhibits a small non linearity of the order of 2%. That non linearity is now understood to be due to the PM response.

4.3 Position dependence of the signals

A good energy resolution, measured in one particular impact point of the calorimeter, is only meaningful if the calorimeter is sufficiently uniform, i.e. if the variation in the average signals measured at random impact points is smaller than the energy resolution. The signal uniformity was studied with electrons from the grid scans. Using the beam chamber measurements and the position of the calorimeter with respect to the beam, the events were subdivided into many different subsets, each containing hits in a very small subarea of the calorimeter (2×2 mm^2). The distribution of the average signals in each of these subsets is given in fig. 8, where the size of the square is a measure for the size of the signal in the subarea concerned. In fig. 9, these data are presented in the form of a histogram. The average signal in each of the subareas corresponds to an entry in this histogram. For the sake of clarity, we have only included electrons entering the central area of the calorimeter, i.e. inside the square formed by the four centers of the four calorimeter towers. Outside this area, lateral shower leakage effects cause decreasing signals. The histogram in fig. 9 is a measure for the nonuniformity of the calorimeter signals. Its RMS width amounts to 2.01 %, which is of the same order as the energy resolution measured in one point (2.09% at 40 GeV). If the points in the boundary region between the modules are removed, the RMS width improves to 1.43%. This result shows that most of the uniformity is due to edge effects in the read-out systems of the 4 calorimeter towers. These effects are well reproduced with measurements performed in the laboratory with a β source. They might be due to local problems in the light collection (like mechanical damage of the fibers during the

bunching, edge effects in light collection and mixing due to the light guide), are subject of further investigation.

4.4 The light yield

The e.m. energy resolution is ultimately limited by the purely statistical fluctuations in the number of charge carriers producing the signal. Since this number is proportional to the energy, the resolution of the calorimeter can be written as

$$\frac{\sigma}{E} = \frac{\sqrt{\sigma^2_{\text{samp}} + \sigma^2_{\text{p.e.}}}}{E} + c \qquad (3)$$

where σ_{samp} describes the sampling fluctuations and $\sigma_{\text{p.e.}}$ the fluctuations due to photoelectron statistics. The contribution of the latter term was determined by measuring the effect of the reduction of the light yield, by means of neutral filters, on the total energy resolution σ/E. These measurements were performed at low energy (20 GeV), in order to limit the contribution of the energy independent term c to the resolution as much as possible. The energy resolutions and the average signals obtained with different filters are listed in table 2.

Since the number of photoelectrons, $N_{\text{p.e.}}$, is equal to $(\sigma_{\text{p.e.}}/E)^{-2}$, (3) can be rewritten as

$$(\frac{\sigma}{E} - c)^2 = (\frac{\sigma_{\text{samp}}}{E})^2 + \frac{1}{f.N_{\text{p.e.}}} \qquad (4)$$

where f, the fraction of light passing the filter, is measured directly from the average response. Figure 10 shows the quantity $(\sigma/E - c)^2$ as a function of $\frac{1}{f}$. The data points correspond to 2 different values of c (see table 2). Indeed, a linear relationship is observed, from which the number of photoelectrons and the sampling term could be determined. The latter is in good agreement with the value found in 4.1. The average number of photoelectrons produced per GeV shower energy (in the absence of neutral filters) amounts to 500 ± 30, where the error is mainly determined by the uncertainty in the contribution of the energy independent term c (see also sect. 4.1).

4.5 The position resolution

The position resolution was determined from the energy sharing between the four calorimeter cells. The center of gravity $(\bar{x}, \bar{y})$ of the energy E_i deposited in the various cells (located at positions (x_i, y_i) with respect to the calorimeter center) contributing to the signal was calculated as

$$\bar{x} = \frac{\sum_i x_i E_i}{\sum_i E_i} \qquad (5)$$

and similarly for the y coordinate. In the following study, we have used the *calorimeter*

axes, rotated by 45 degrees with respect to the *laboratory* axes, in order to preserve the natural sharing of the energy among the cells.

It is well known that the impact point calculated in this way tends to be systematically shifted towards the center of the cell hit by the particle[13,21,22,23] . This is illustrated in fig. 11a, in which the $\bar{x}$ coordinates are compared to the real impact points, given by the $x_{\rm BC}$ coordinates derived from the beam chamber data. Only in the center of a cell and near the boundaries between different cells is the impact point correctly determined. One may solve this problem either by giving a larger weight to cells with a small energy deposit in calculating the center of gravity, or by shifting the center of gravity found by (5) using an empirical algorithm. The latter procedure was chosen in this analysis. The reconstructed impact point $(\bar{x}, \bar{y})$ was shifted to the approximately correct position in the following way:

$$\bar{x}_{\rm corr} = 2.53 \ \tan(0.075\bar{x}) \ \ {\rm mm} \qquad (6a)$$

$$\bar{y}_{\rm corr} = 2.68 \ \tan(0.074\bar{y}) \ \ {\rm mm} \qquad (6b)$$

The relation between the real impact points $x_{\rm BC}$ and the reconstructed ones $\bar{x}_{\rm corr}$ is shown in fig. 11b. The points in this scatter plot cluster around the line $x_{\rm BC} = \bar{x}_{\rm corr}$, which shows that the method works well. One can notice that this correction works better one the negative x side of the calorimeter (see fig. 11b). This is due to the fact that the shower is better contained in that case. When sending the beam on the other side, one would need the information from extra neighboring modules in calculating the barycenter of the shower.

The experimental data entering the scatter plots of fig. 11 were taken from the grid scan at 40 GeV, in which the central area of the calorimeter was rather uniformly covered with electron hits. Similar data were taken at 20 GeV. The correction formulae (6) worked equally well at that energy.

Since these results are obtained from a comparison between the particle's coordinates derived fom the calorimeter data and from the hits in the beam chambers, the inaccuracy of the latter also contributes to the measured position resolution. This contribution, estimated to be ~ 340 μm, has been unfolded in what follows. The x-position resolution, given by the width of the band in fig. 11, is shown in fig. 12. The distribution of the quantity $(x_{\rm BC} - \bar{x}_{\rm corr})$ is found to be a gaussian, its width varying with the impact point. The best resolution (0.45 mm) is observed at the boundaries between modules where the energy sharing is optimal. The worst resolution (1.5-2.5 mm) is obtained at the center of the cells where the energy sharing is less favorable and also where one would need the information from extra neighboring modules. The asymmetry of the distribution in fig. 12 is a consequence of the tilt of the beam towards the positive x-axis leading to a worse shower containment for $x \geq 0$. From this figure, we conclude that the position

resolution, averaged over the detector surface, amounts to 1 mm at 40 GeV. Similar results were obtained for the y coordinate.

For other energies, only data in the vicinity of the center of the calorimeter were available. The position resolution in this area is shown as a function of energy in fig. 13. This data is adequately described by the following expression

$$\sigma_x = \frac{1.8 \text{ mm}}{\sqrt{E}} + 0.10 \text{ mm} \tag{7}$$

with E in GeV. We obtained similar results for the y coordinate. As pointed out before, the position resolution averaged over the whole calorimeter is about 2.5 times worse. One can note that the resolution found at 40 GeV is 0.35 mm, lower than the one quoted above (0.45 mm) which is the x position resolution averaged over all values of y. Since the beam enters the calorimeter at an angle, the fluctuations in depth of the shower development show up in the constant term of (7). As a check, we also studied the position resolution as a function of the energy in the *laboratory* axes. The scaling term found both for x and y is the same as in (7). While a constant term $\simeq 0.13$ mm is found in x, no constant term is found in y where the tilting angle is zero.

4.6 Particle separation in space

Particle-particle separation may be an important issue for future collider experiments. Whereas charged particles can be easily distinguished from one another by means of a tracking system, calorimetry is the only option for neutral particles. An important background to single-photon production, which is often an interesting event signature (as in the $H \rightarrow \gamma\gamma$ issue), comes from $\pi^0 \rightarrow \gamma\gamma$ decay in which the two γ's are not resolved by the detector.

The space separation of two e.m. showers was studied with a method previously employed in ref. 13. Electrons entering the detector in its central region were used to define an average shower profile, i.e. average values for the fractions of the shower energy deposited in each of the four cells, $\bar{f}_i$. For individual events, the quantity K is defined, which determines how well the event is described by this average profile:

$$K = \sum_i r_i \times (f_i - \bar{f}_i)^2 \tag{8}$$

where r_i is the distance between the center of module i and the shower barycenter. One may also determine K for the superposition of two e.m. showers developing in different parts of the calorimeter. The accuracy in the particle-particle separation is then determined by the fraction of such events passing a cut in K, which eliminates (almost all) the single shower events.

The 40 GeV electrons from the grid scan were used for this analysis. The reference profile $\bar{f}_i$ was determined from 80 GeV electrons entering the central detector region at $\theta_z = 2^0$. This profile was compared to energy distributions obtained by superimposing the signals from two 40 GeV electrons hitting the detector at positions with a relative distance d and whose center of gravity is in the detector center. Figure 14 shows the distributions for the 80 GeV electron showers and for the superimposed 40 GeV ones, for a distance d = 15 mm between the 2 electrons. A cut on the value of K gives the probability for misidentifying a pair of showers as a single shower, for a given efficiency of recognizing the single shower as such. These probabilities are given in fig. 15, where the probability for misidentifying a shower pair is shown as a function of d, for various single-shower efficiency. Extrapolating from this figure, we conclude that π^0's can be reasonably recognized and distinguished from single photons if the two γ's from π^0 decay are separated by at least 20 mm. The γ's from the decays of π^0's forming the dominant background to the signal from a 100 GeV $H \rightarrow \gamma\gamma$ decay process are spatially separated by typically 5-6 mm, for a calorimeter starting at 1.5 m from the vertex. In that case a rejection factor of 1.7 is obtained, for 90% electron efficiency.

4.7 Measurements on pions

The detector that is subject of this paper is primarily intended for e.m. shower detection. It may, however, also serve as the e.m. section of a calorimeter system that is used for hadron detection. In that case, one may ask the question to what extent the bunch of fibers sticking out at the rear end of the e.m. section affects the signals from hadron showers, which are only partially contained in this section. Several earlier studies reported significant effects for electrons[18] (for shorter calorimeters than the present one) and muons[14] due to anomalous sampling in this readout area.

In order to determine the possible contribution of such effects for hadronic shower signals, we made a comparitive measurement of 150 GeV π^- at $\theta_z = 2^0$ and at $\theta_z = 182^0$. In the latter case the pions entered the detector from the rear end, so any effects of shower particles leaking out longitudinally should not contribute to the signal, in contrast to what happens for $\theta_z = 2^0$. In fig. 16, the two signal distributions are shown together after removing the contribution of the non-interacting pions in the calorimeter by requiring a deposited energy larger than 20 pC. They are practically identical and the difference of their mean value is consistent with what is expected from the finite attenuation length contribution. In particular, there is no evidence for a high-energy tail in the $\theta_z = 2^0$ distribution. Similar results were obtained for 20 GeV pions. From these data we can conclude that this calorimeter could be used as the e.m. section of a high-performance calorimeter system without spoiling the hadron/jet resolution.

5. *SUMMARY AND CONCLUSIONS*

A very fine-sampling electromagnetic calorimeter consisting of 0.5 mm thick plastic scintillating fibers embedded in lead has been tested. Because of the large fraction of high-Z absorber material ($\sim$ 78% in volume), this detector is extremely compact, with an effective radiation length of only 7.2 mm. The energy resolution for electron detection was measured to be $9.2\%/\sqrt{E(GeV)}$, plus a small energy independent term, which is determined by the angle θ_z between the particle's direction and the fiber axis. For $\theta_z = 2^0$, this term amounts to about 0.6% and for larger angles it becomes even smaller. In spite of the small sampling fraction (only 3.5% for mip's), photon statistics do not limit the performance of this detector. The signals are produced by $\sim$ 500 photoelectrons for each GeV of energy deposited in the calorimeter, so that photon statistics contribute $4.5\%/\sqrt{E}$ (in quadrature) to the energy resolution. Therefore, a further reduction of the fiber diameter may result in even better energy resolutions.

The calorimeter exhibits signal nonuniformities at the level of 2%. However, these nonuniformities occur systematically near the boundaries between different calorimeter towers and, therefore, one may apply corrections eliminating them in the same way as nonuniformities in the light collection of crystal calorimeters (NaI, CsI, BGO, etc.) are dealt with. Such position dependent corrections obviously benefit from a good position resolution. A position resolution of $1.8\text{mm}/\sqrt{E(GeV)}$ was measured at the junction of the four 4 × 4 cm^2 cells of the calorimeter. This corresponds to 0.03 × 0.03 in $\Delta\eta \times \Delta\phi$ units if the calorimeter were to be located at a realistic distance of $\sim$ 1.3 m from the interaction vertex in a collider experiment. Thanks to the small Molière radius and the fine granularity, two e.m. showers could be seen as separated at relative distances down to $\sim$ 20 mm in more than 90 % of the cases.

Measurements on pions showed no significant differences between the signals from particles entering the detector through the front or the back face. Therefore, we conclude that the fibers sticking out at the rear should not be a disturbing factor for the hadronic performance of a longitudinally segmented calorimeter of this type.

In an effort to further improve the performance of this detector, we are presently building e.m. modules with 1 mm diameter fibers and a lead to fiber ratio of 1.8:1 in volume, which will operate with an incident angle $\theta_z \simeq 6^0$. A sampling term of $\simeq$ 9% and a constant term of $\simeq$ 0.2% in the energy resolution are expected for such a calorimeter according to simulations[19].

Acknowledgements

The work described in this paper would have been impossible without the outstanding technical support provided by our engineers and technicians M. Billault, S. Bricola,

B. Canton, J.-M. Chapuis, J-C. Clémens, P. Clément, M. Commerçon, M. Crouau, F. Daudon, J-J. Destelle, C. Farella, B. Foligne, A. Freddi, D. Imbault, G. Improta, G. Iuvino, P. Laloux, F. Pagano, R. Pirard, P. Repain, R. Rocco, L. Rose-Dulcina, R. Saigne, D. Sauvage, and C. Schillinger. Financial support from the Istituto Nazionale di Fisica Nucleare to the Napoli and Pavia groups, from the Junta Nacional de Investigaçao Científica of Portugal to the Lisbon group, from the Conselho Nacional de Desenvolvimento Cientifico e Tecnologico of Brazil to the Rio de Janeiro group, from the Institut National de Physique Nucléaire et de Physique des Particules, and from the U.S. Department of Energy and National Science Foundation to the San Diego group is acknowledged. One of us (F.R.) would like to thank the Digital Equipment Corporation for support. And finally, we are grateful to the staff of the SPS, and in particular to N. Doble, for the excellent beam conditions and assistance provided during our tests.

REFERENCES

1. F.G. Hartjes and R. Wigmans, Nucl. Instr. and Meth. **A277** (1989) 379.
2. D. Acosta *et al.*, Nucl. Instr. and Meth. **A302** (1991) 36.
3. D. Acosta *et al.*, Nucl. Instr. and Meth. **A314** (1992) 432.
4. D. Acosta *et al.*, Nucl. Instr. and Meth. **A309** (1991) 143.
5. D. Acosta *et al.*, Nucl. Instr. and Meth. **A316** (1992) 184.
6. D. Acosta *et al.*, Nucl. Instr. and Meth. **B62**(1991), 116.
7. A. Simon (WA89 Collaboration), Detecting and triggering on neutrons using the SPACAL Pb/sintillating-fiber calorimeter, contribution to the 2nd Int. Conf. on Calorimetry in High Energy Physics, Capri (I), 1991.
8. R. Wigmans, Nucl. Instr. and Meth. **A259** (1987) 389.
9. D. Acosta *et al.*, Nucl. Instr. and Meth. **A308** (1991) 481.
10. The GEM Collaboration, Letter of Intent for an Experiment at the SSC (1991).
11. The ATLAS Collaboration, Letter of Intent for an Experiment at the LHC (1992).
12. The CMS Collaboration, Letter of Intent for an Experiment at the LHC (1992).
13. D. Acosta *et al.*, Nucl. Instr. and Meth. **A305** (1991) 55.
14. D. Acosta *et al.*, Nucl. Instr. and Meth. **A320** (1992) 128.
15. D. Hertzog *et al.*, Nucl. Instr. and Meth. **A294** (1990) 446.
16. H. Burmeister *et al.*, Nucl. Instr. and Meth. **A225** (1984) 530.
17. We define the nuclear interaction length λ_I in the same way as the Particle Data Group in Phys. Lett. **B239** (1990), page III 5,6. It is the mean free path for *protons* between inelastic interactions. Since the inelastic cross sections for pions are $\sim 50\%$ larger, $\lambda_\pi \approx 1.5\lambda_I$.
18. D. Acosta *et al.*, Nucl. Instr. and Meth. **A294** (1990) 193.
19. R. Wigmans, Performance and Limitations of Hadron Calorimeters, Proc. of the 2nd Int. Conf. on Calorimetry in High Energy Physics, Capri (I), 1991; preprint CERN-PPE/91-205 (1991).
20. Particle Data Group, Phys. Lett. **B239** (1990) page III 5,6.
21. G.A. Akopdjanov *et al.*, Nucl. Instr. and Meth. **140** (1977) 441.
22. R.L. Carrington *et al.*, Nucl. Instr. and Meth. **163** (1979) 203.
23. S. Orito and T. Kobayashi, Nucl. Instr. and Meth. **215** (1983) 93.

FIGURE CAPTIONS

1. The structure of the fiber calorimeter. Shown are the lateral stucture of the calorimeter as a whole (a) and a detail of the front face (b).
2. Layout of the beam line, seen from above. In our convention, the angle θ_z shown in this figure has a positive sign. See text for details.
3. Signal distributions of 40 GeV electron showers measured at different angles (θ_z) between the particle's direction and the fiber axis.
4. The energy resolution for electrons as a function of the square-root of energy, for $\theta_z = 2^0$. The lines are the results of fits to the experimental data.
5. The constant term in the e.m. energy resolution as a function of the angle θ_z between the particle direction and the fiber axis, for 40 GeV electrons.
6. The average calorimeter signal per unit of energy, normalized to 1 at 40 GeV, for electrons entering the detector at an angle $\theta_z = 2^0$. Results are given before and after correcting for the effects of light attenuation in the fibers. Also shown the 2 hyperbolae corresponding to the uncertainty in the beam energy due to hysteresis.
7. The signal for 40 GeV electrons entering the calorimeter perpendicularly ($\theta_z = 90^0$), as a function of the distance of the impact point from the calorimeter front face.
8. The nonuniformity of 40 GeV electron signals. Each square represents the average signal for electrons entering the detector in that particular area.
9. The nonuniformity of the electron signals. Each entry in the histograms represents the average calorimeter signal for 40 GeV electrons, measured in a different region with a diameter of 2 mm. Data taken at $\theta_z = 2^0$.
10. The scaling term of the energy resolution for 20 GeV electrons as a function of the average calorimeter signal, obtained from measurements with different neutral filters. The abscissa is linear in the inverse of the filter transmission. The two sets of experimental points correspond to two extreme choices for the contribution of the energy independent term c to the measured energy resolution (Fig. 4).
11. Scatter plots for 80 GeV electrons, showing the x-coordinate of the impact point measured with the beam chambers versus the x-coordinate determined from the calorimeter data with the center-of-gravity method. Results are shown before (a) and after (b) correcting for the systematic displacement effects inherent to this method, with formula (6). Data taken at $\theta_z = 2^0$.
12. The position resolution for 80 GeV electrons, after unfolding the beam chamber resolution, as a function of the position in the detector. The point (0,0) corresponds to the center of the 4 cells. Data taken at $\theta_z = 2^0$.

13. The position resolution for electrons at $\theta_z = 2^0$ as a function of energy, for particles sent at the junction of the four cells of the calorimeter, after unfolding the beam chambers resolution. Averaged over the whole detector, the results are 2.5 times worse.

14. Distribution of the spatial parameter K, which determines how well the shower profile of an individual event is described by the average profile. Results for 80 GeV electrons and for 40 GeV electron pairs. The two electrons are separated by 15 mm.

15. The probability for misidentifying an electron pair (40 + 40 GeV) as a single 80 GeV e.m. shower, as a function of the distance between the two electrons. Values are shown for electron efficiency of 90 % (closed circles) and 72 % (open circles).

16. Signal distributions for 150 GeV π^- entering the e.m. fiber calorimeter at $\theta_z = 2^0$ (a) and $\theta_z = 182^0$ (b).

TABLE CAPTIONS

1. Energy resolution and signal linearity for electrons. Listed are the beam energy, the average signal and the energy resolution as measured from the raw data, and the average signal per unit of energy, normalized to 1 at 40 GeV.
2. Determination of the light yield of the calorimeter. Listed are for each neutral filter the measured transmission coefficient f, the energy resolution for 20 GeV electrons, the average calorimeter signal and the squared energy resolution obtained after subtracting the energy independent term c. For the latter, we chose values of 0.5% and 0.75%, respectively, which may be considered as extreme cases (see sect. 4.1.2).

Table 1 Electron resolution and linearity ($\theta_z = 2^0$)			
E(GeV)	<signal>$_{\text{meas}}$(pC)	$(\sigma/E)_{\text{meas}}$(%)	<signal/E>
9.6	38.43±0.04	3.80±0.03	1.000±0.001
20	79.55±0.04	2.64±0.02	0.995±0.001
40	159.97±0.23	2.09±0.02	1.000
80	325.67±0.13	1.63±0.02	1.018±0.001
150	619.88±0.23	1.44±0.03	1.033±0.002

Table 2 Light yield					
Filter	f_{measured}	σ/E (%)	<Signal> (pC)	$(\sigma/E - c_1)^2$	$(\sigma/E - c_2)^2$
NO	1	2.73	76.90	$4.97\ 10^{-4}$	$3.92\ 10^{-4}$
1	0.268	3.24	20.24	$7.51\ 10^{-4}$	$6.20\ 10^{-4}$
2	0.161	3.74	12.15	$10.50\ 10^{-4}$	$8.94\ 10^{-4}$

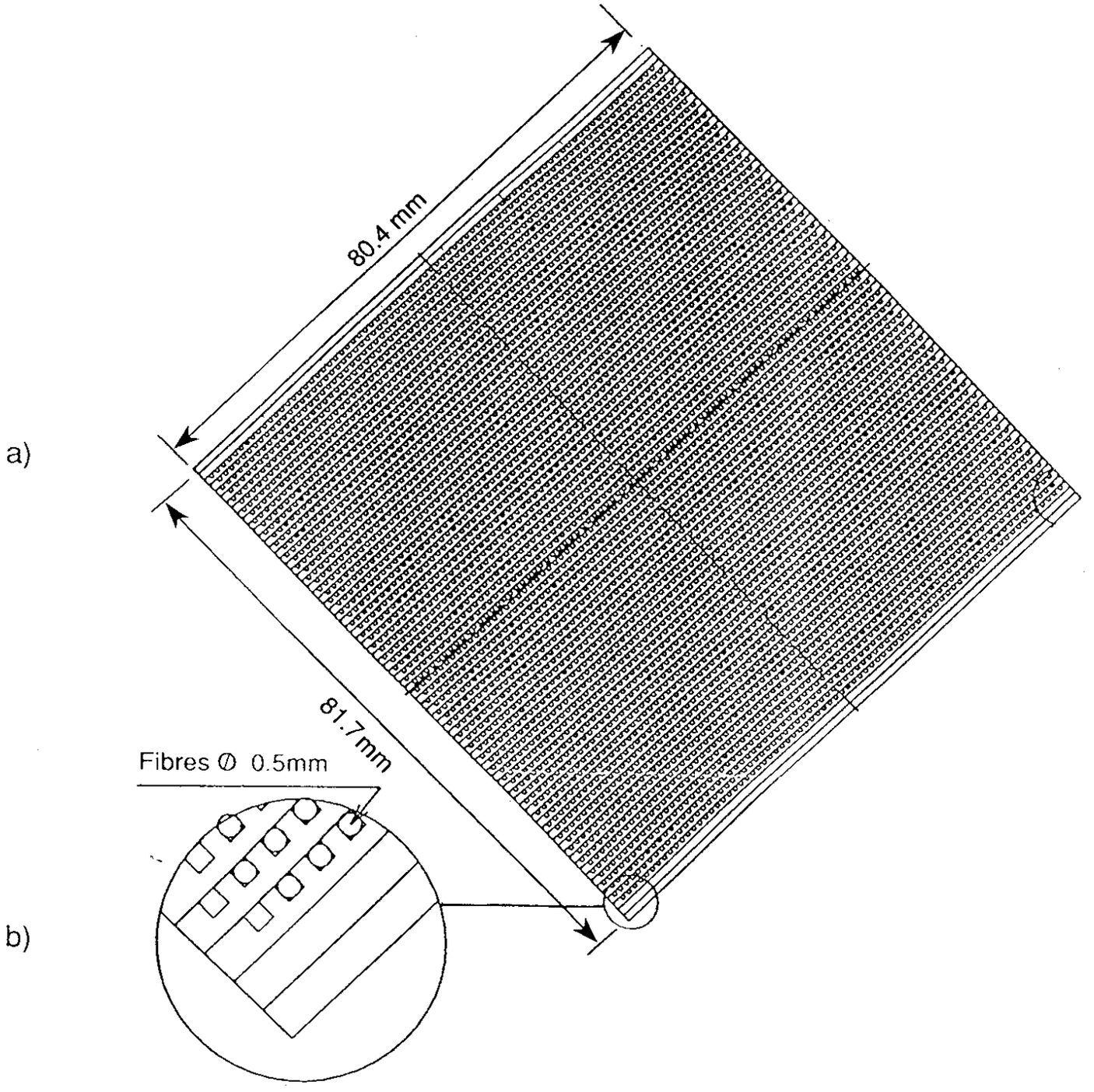

Fig. 1

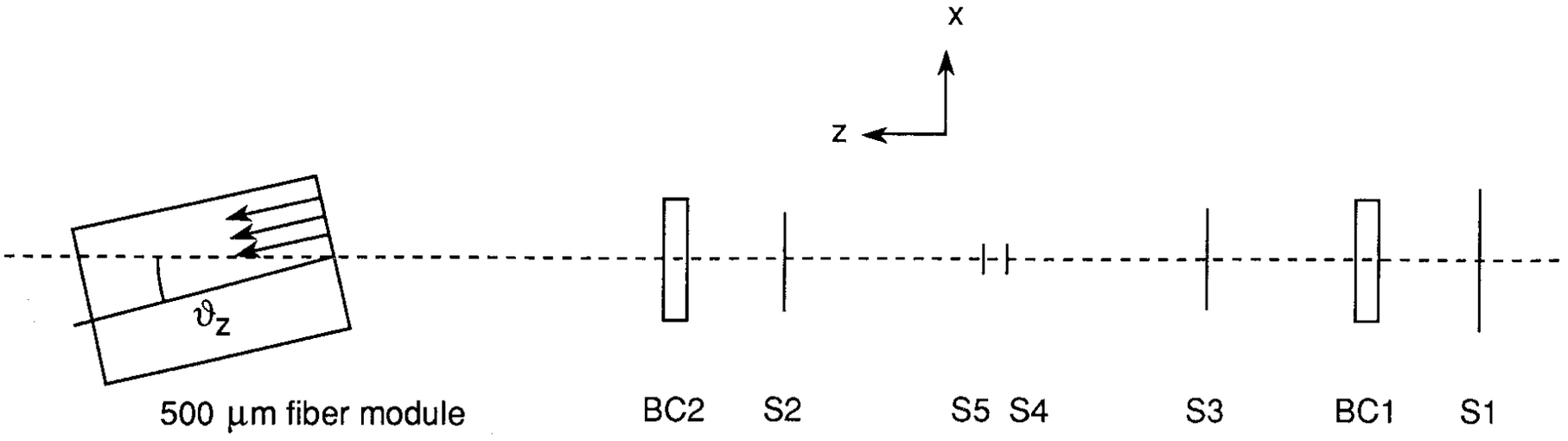

Fig. 2

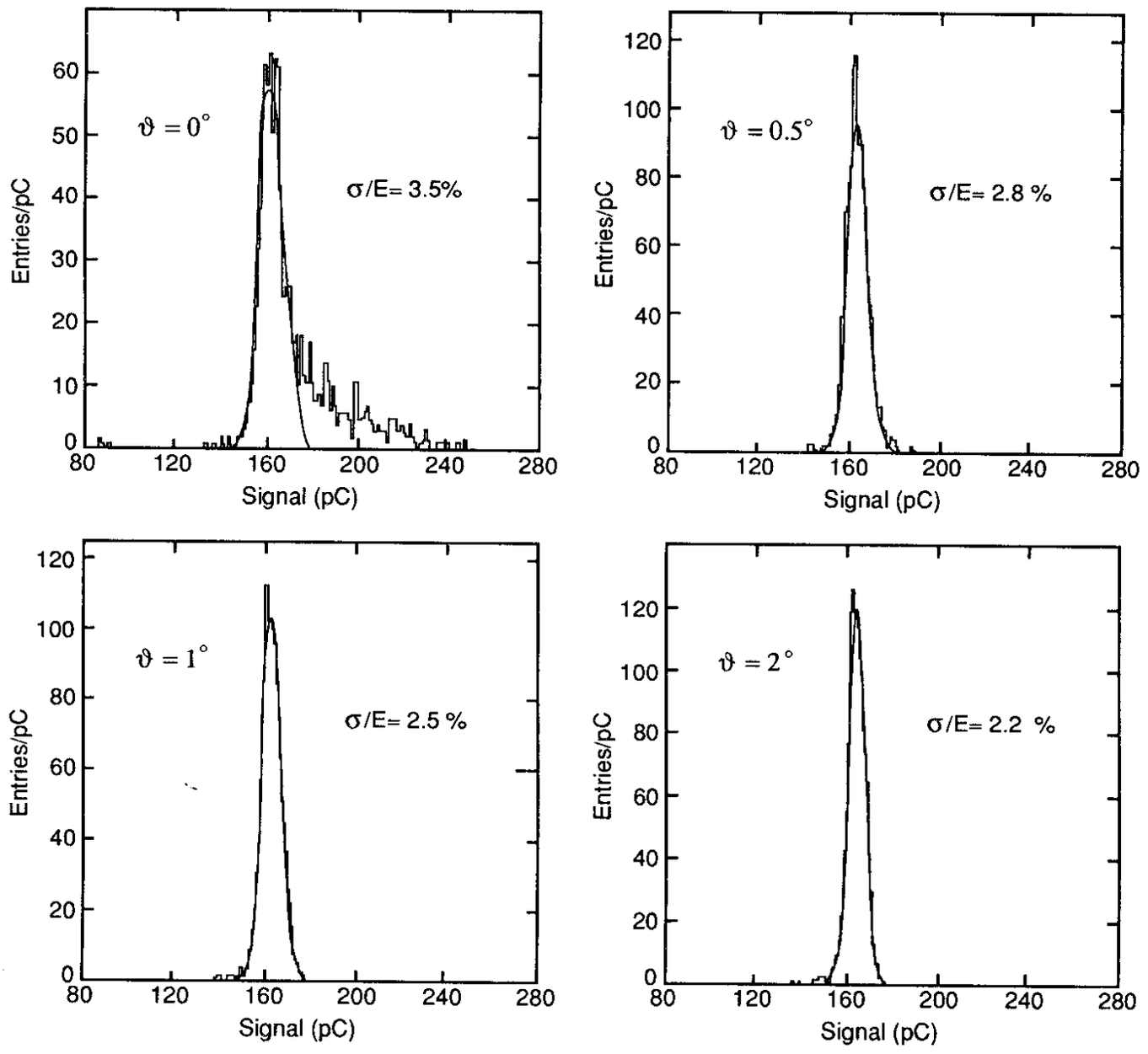

Fig. 3

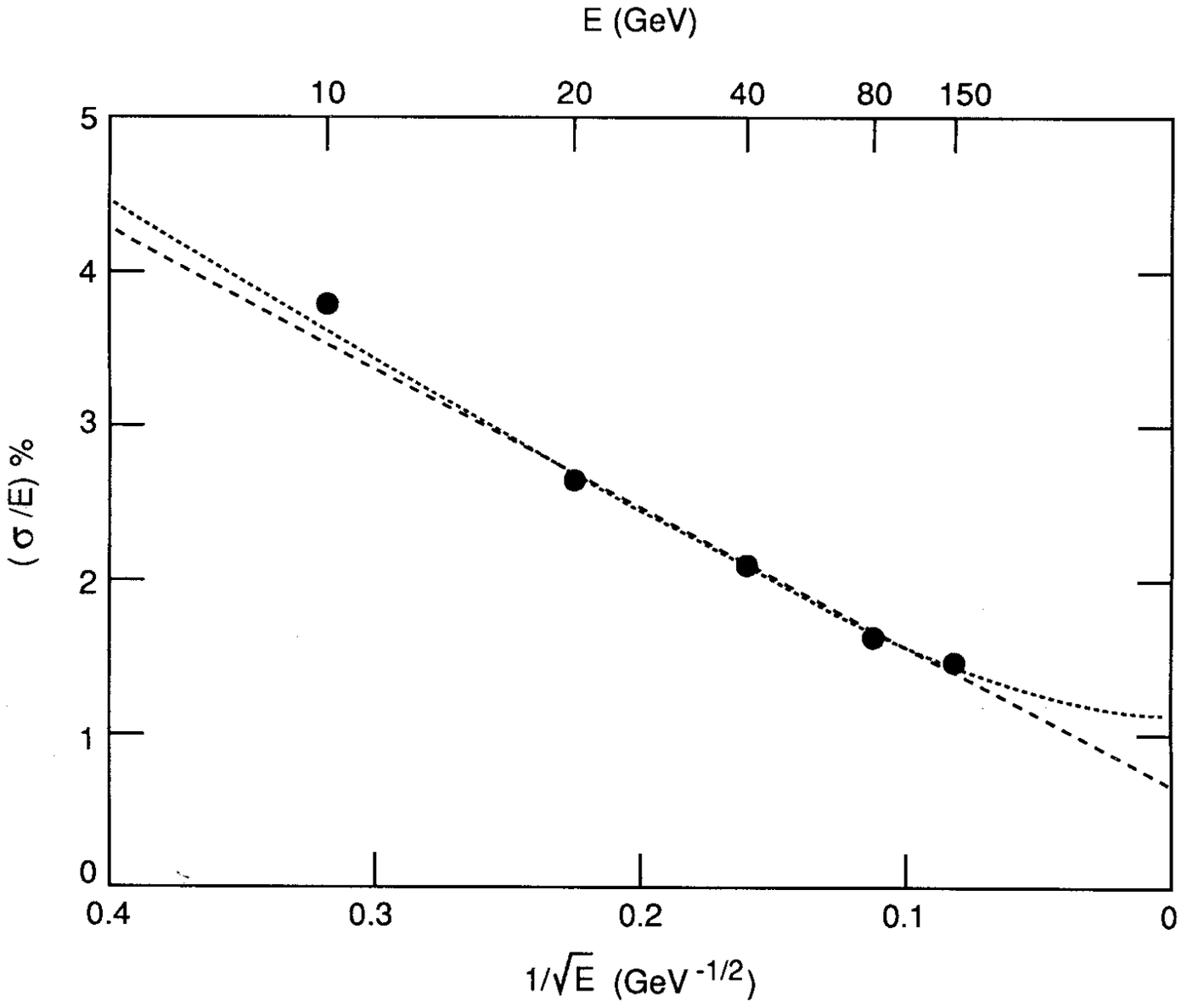

Fig. 4

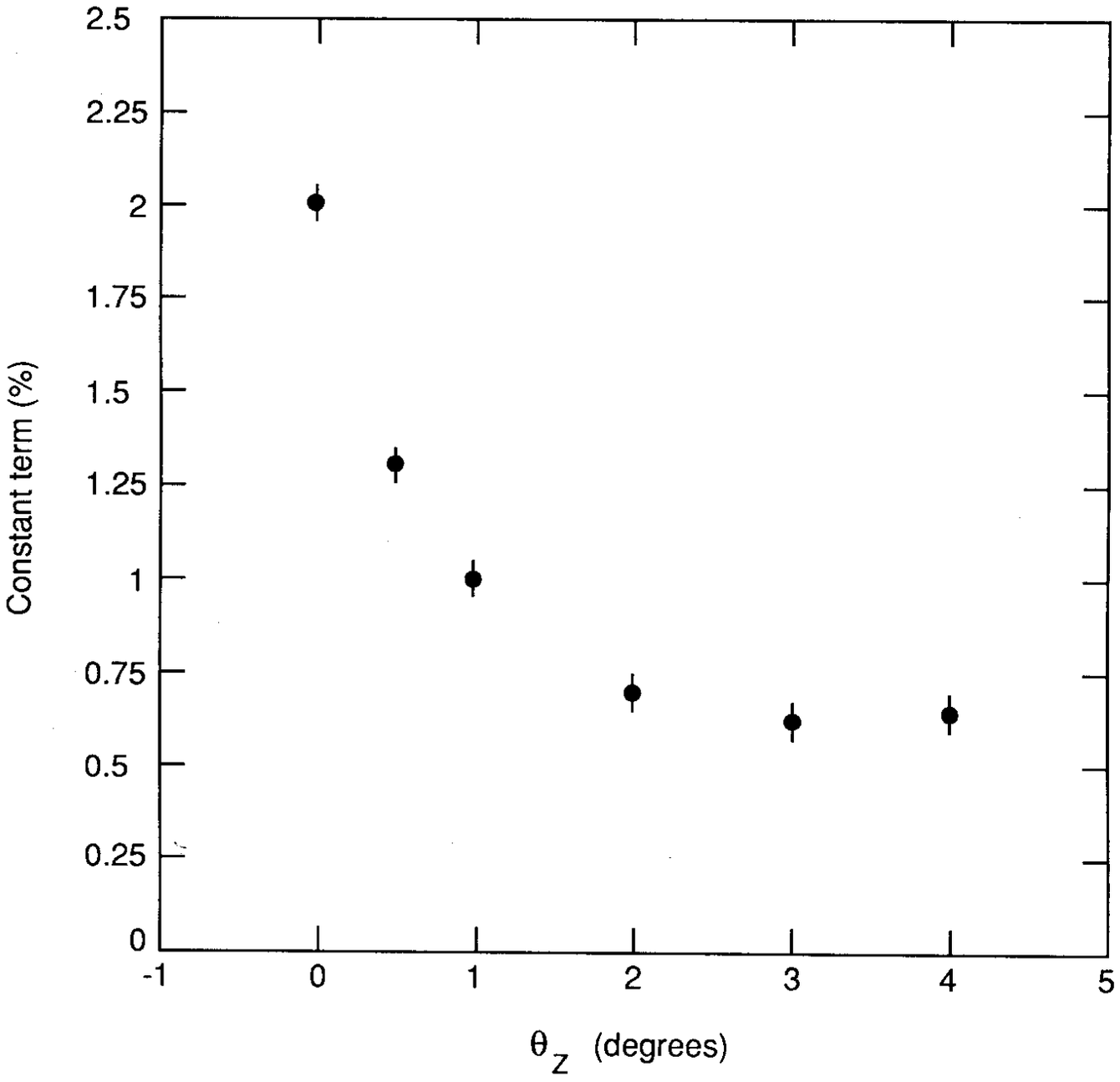
2.5
2.25
2
1.75
1.5
1.25
1
0.75
0.5
0.25
0
Constant term (%)
-1
0
1
2
3
4
5
θ Z (degrees)

Fig. 5

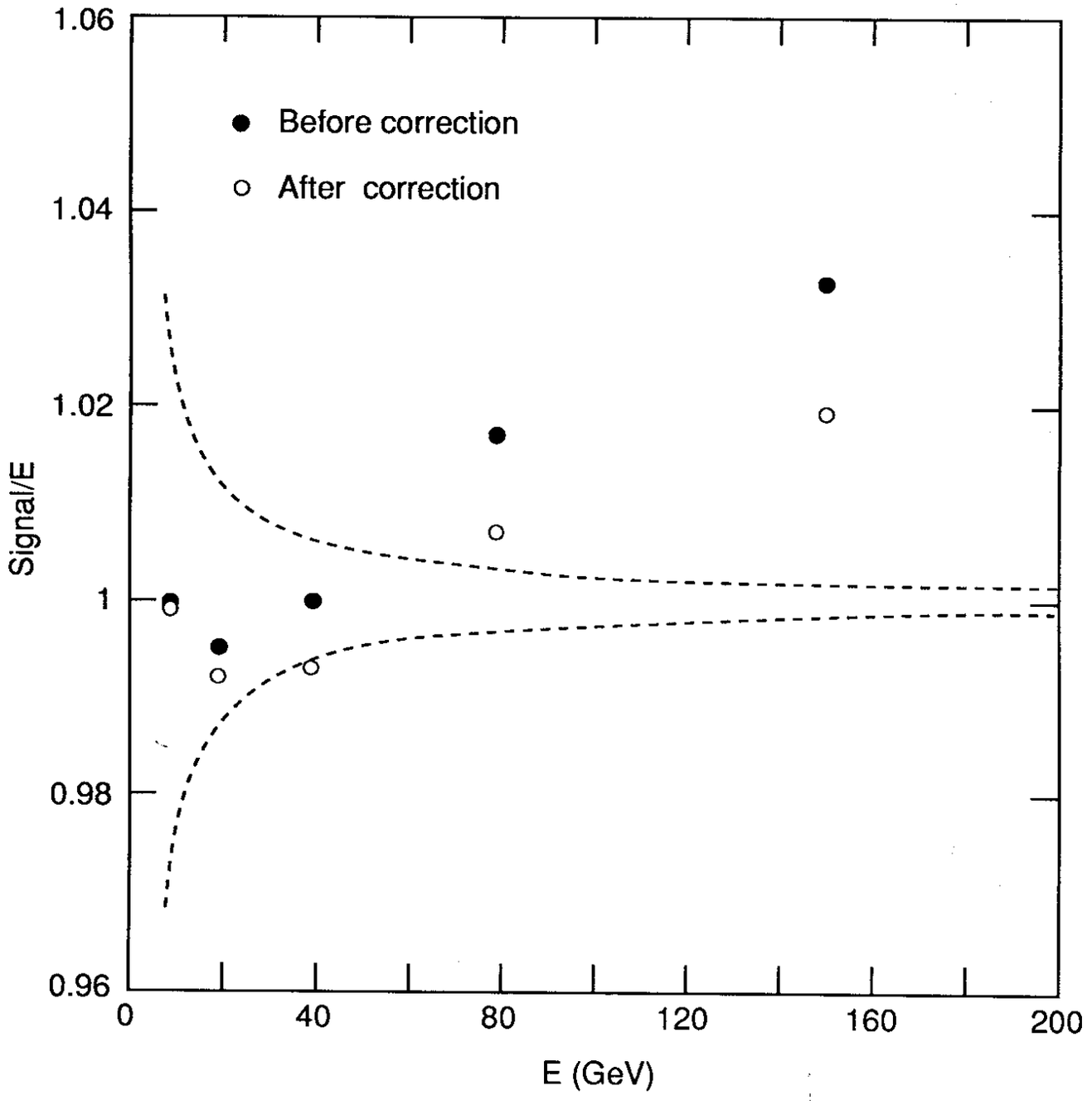
1.06
1.04
1.02
1
0.98
0.96
Signal/E
Before correction
After correction
0
40
80
120
160
200
E (GeV)

Fig. 6

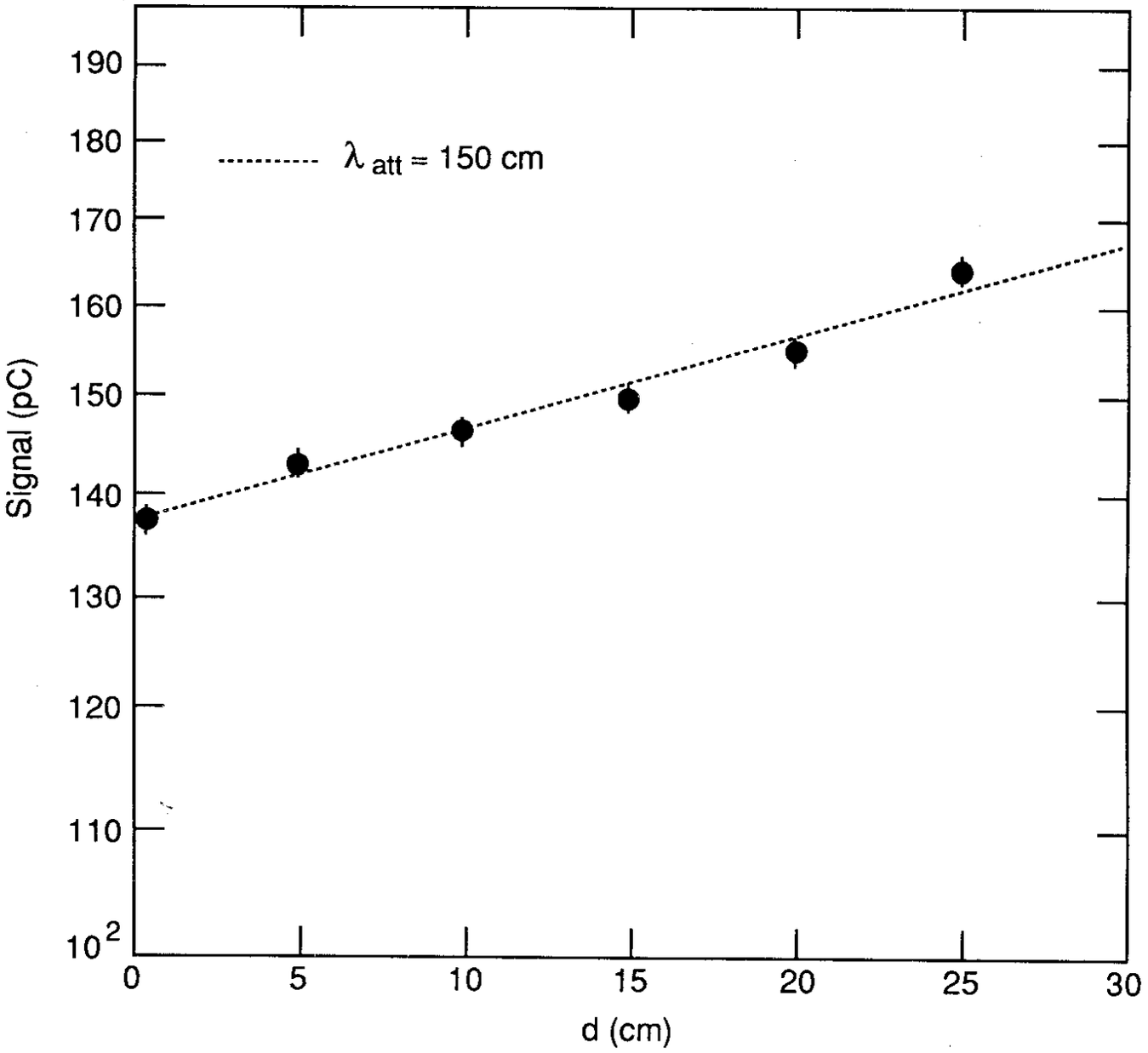
190
180
170
160
150
140
130
120
110
10^2
Signal (pC)
λ_{att} = 150 cm
0
5
10
15
20
25
30
d (cm)

Fig. 7

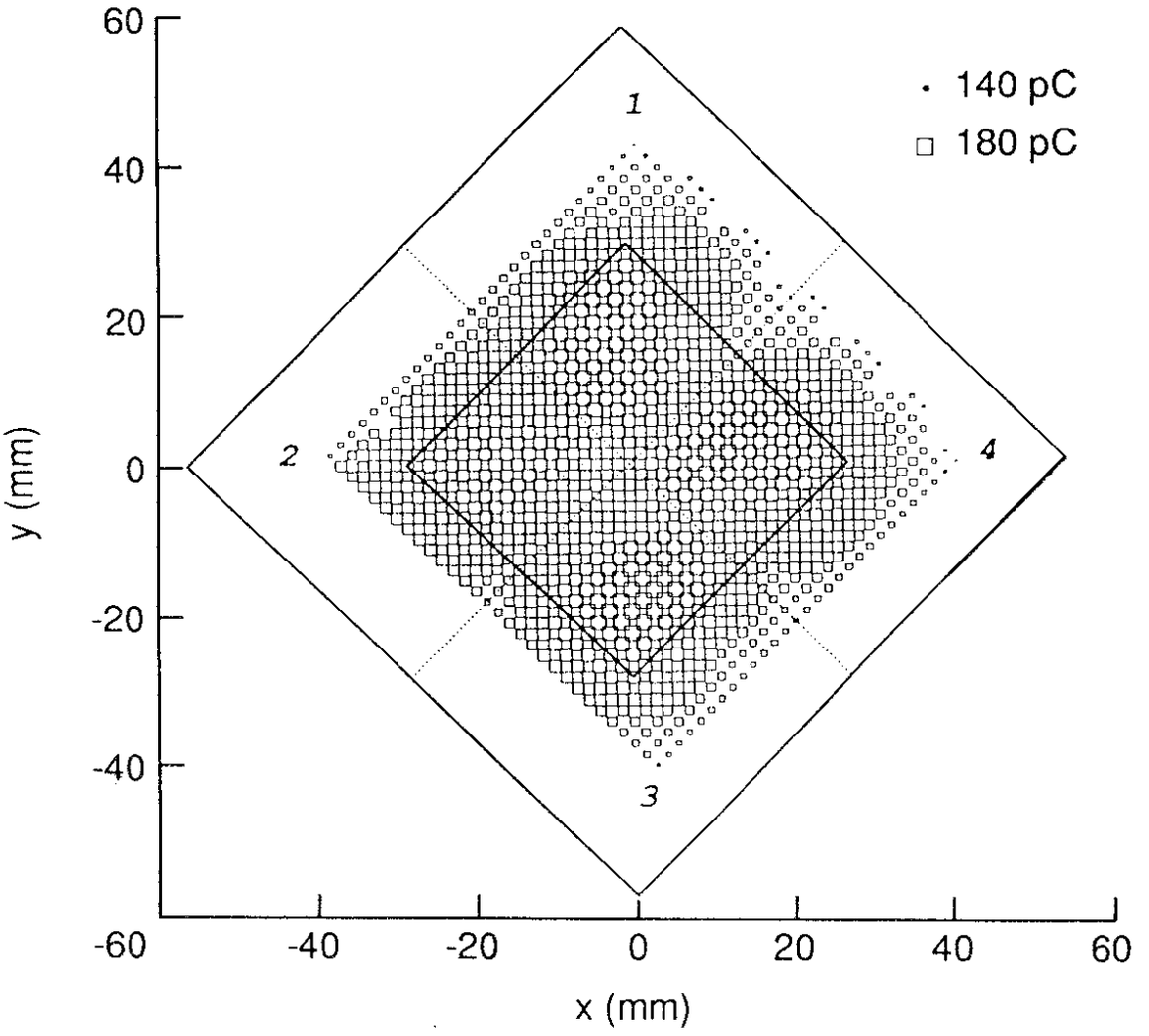

Fig. 8

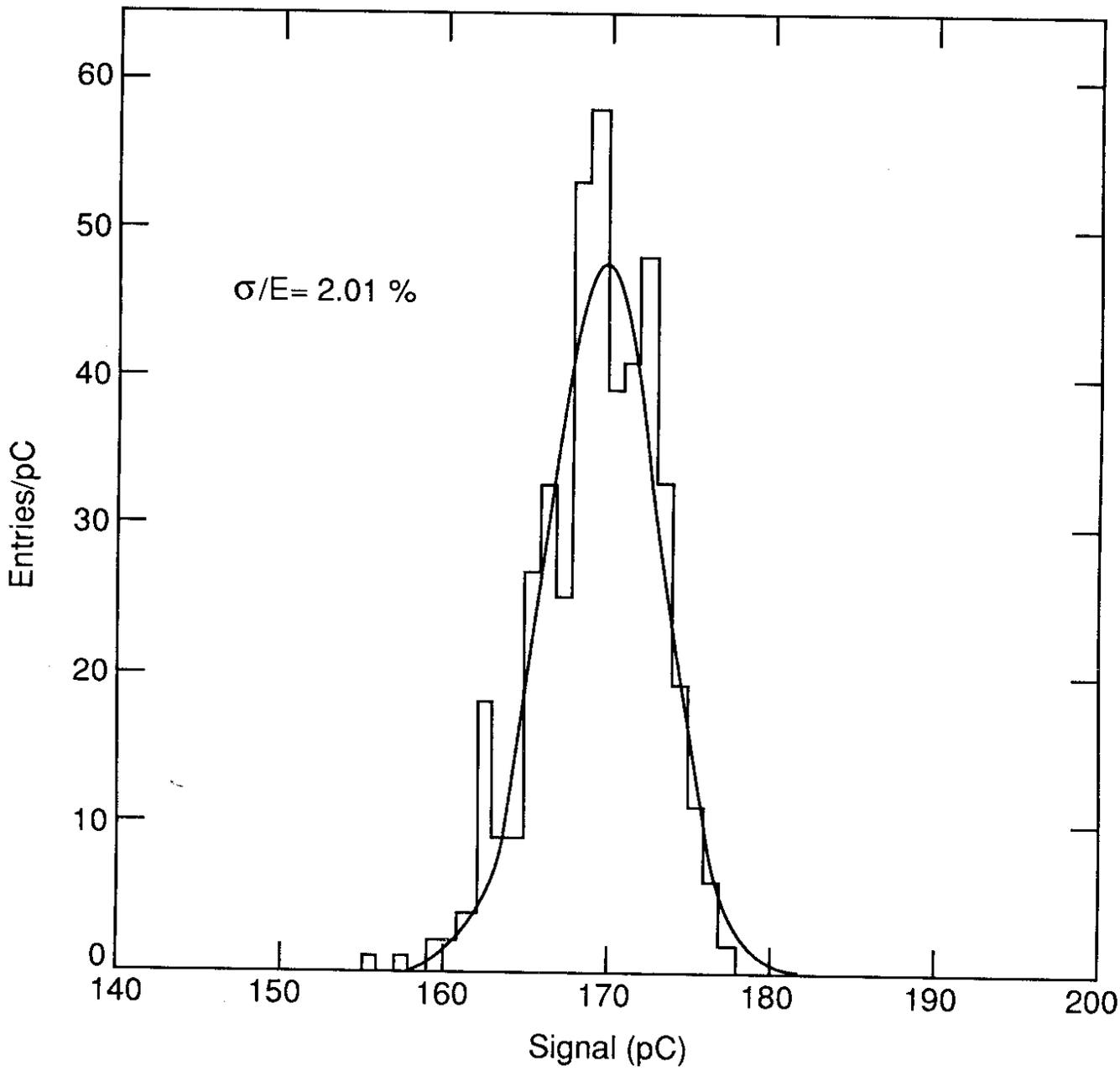
σ/E= 2.01 %
Entries/pC
Signal (pC)
0
10
20
30
40
50
60
140
150
160
170
180
190
200

Fig. 9

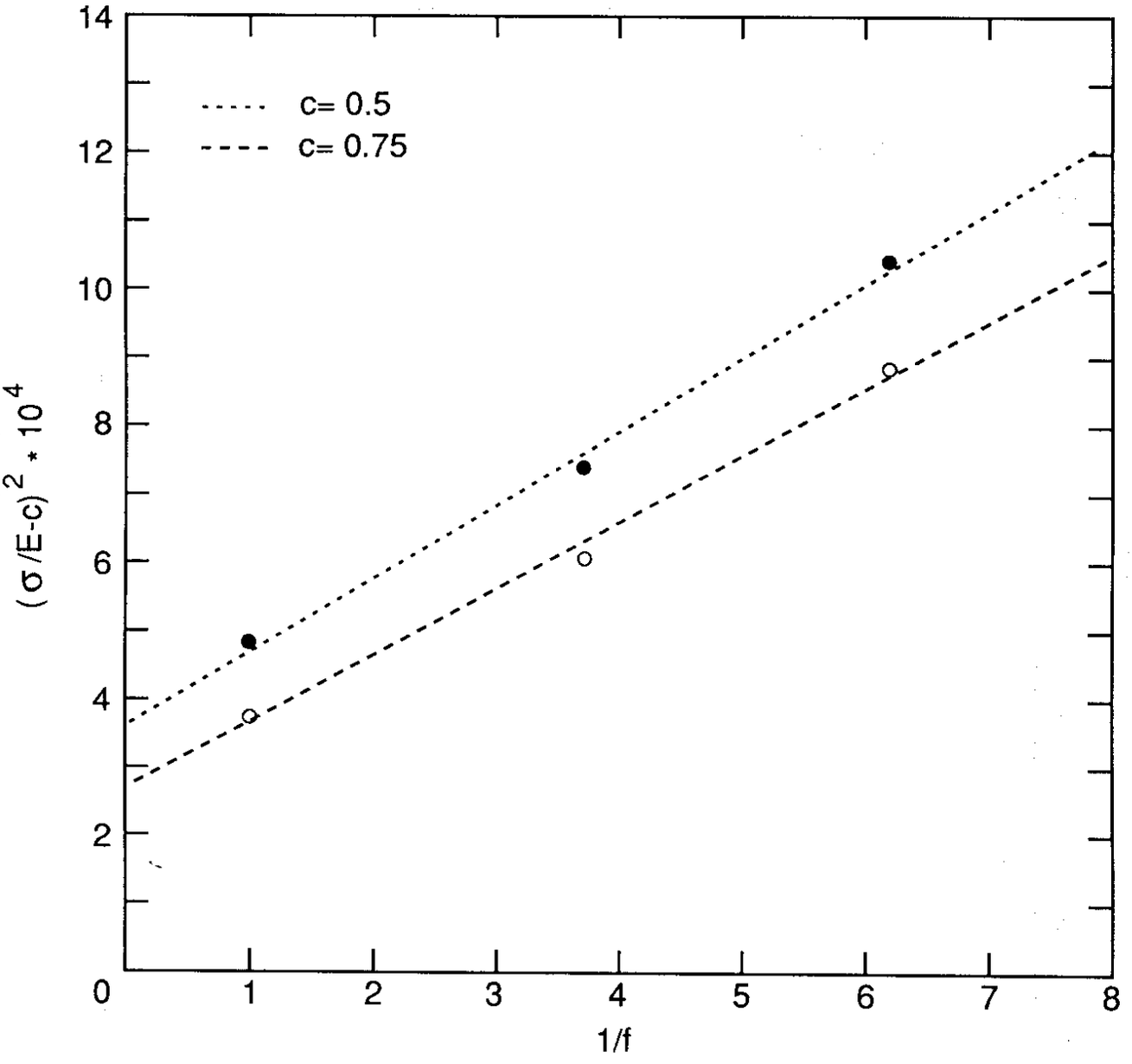

Fig. 10

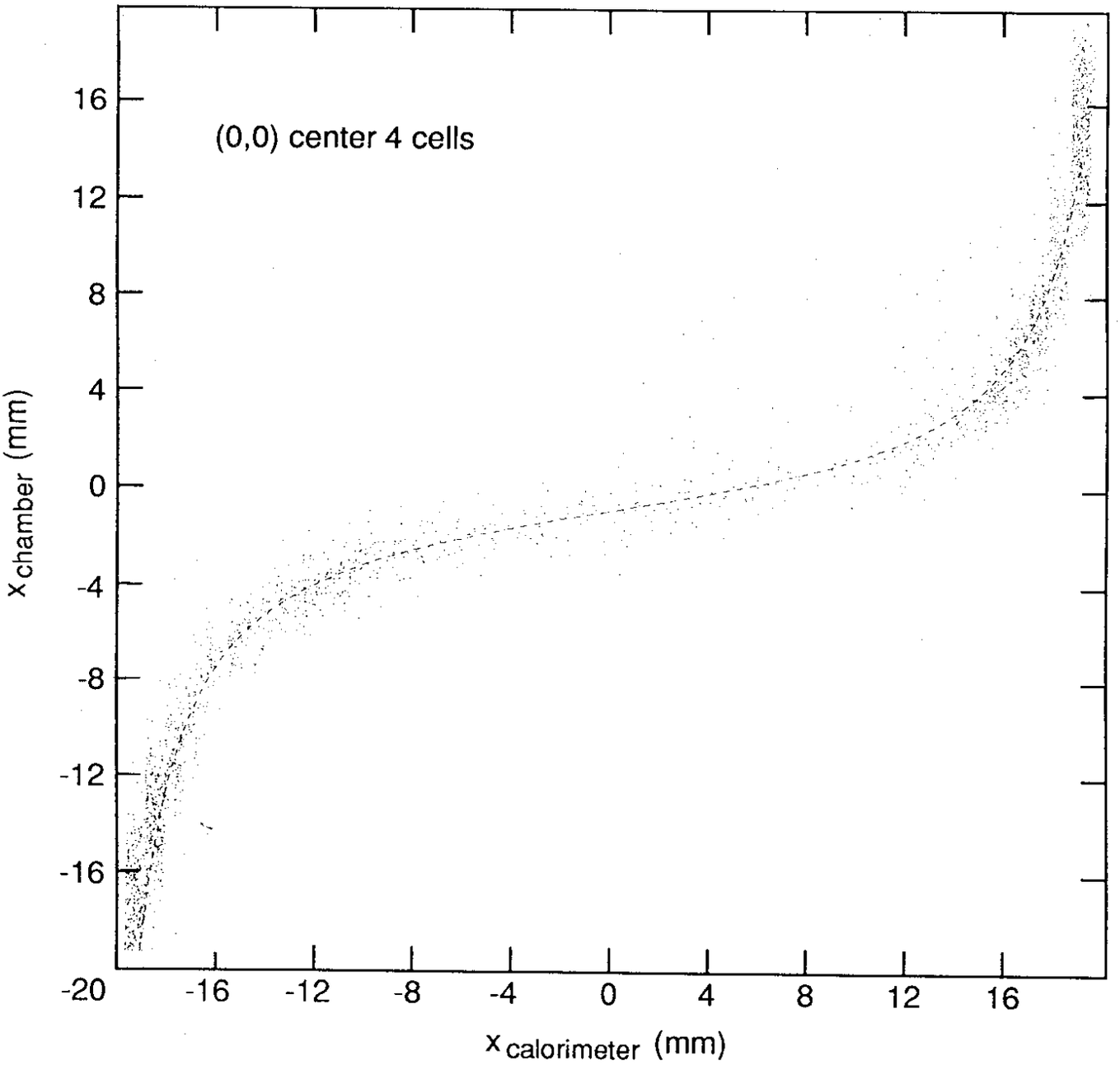
(0,0) center 4 cells
16
12
8
4
0
-4
-8
-12
-16
-20
-16
-12
-8
-4
0
4
8
12
16
x chamber (mm)
x calorimeter (mm)

Fig. 11 a)

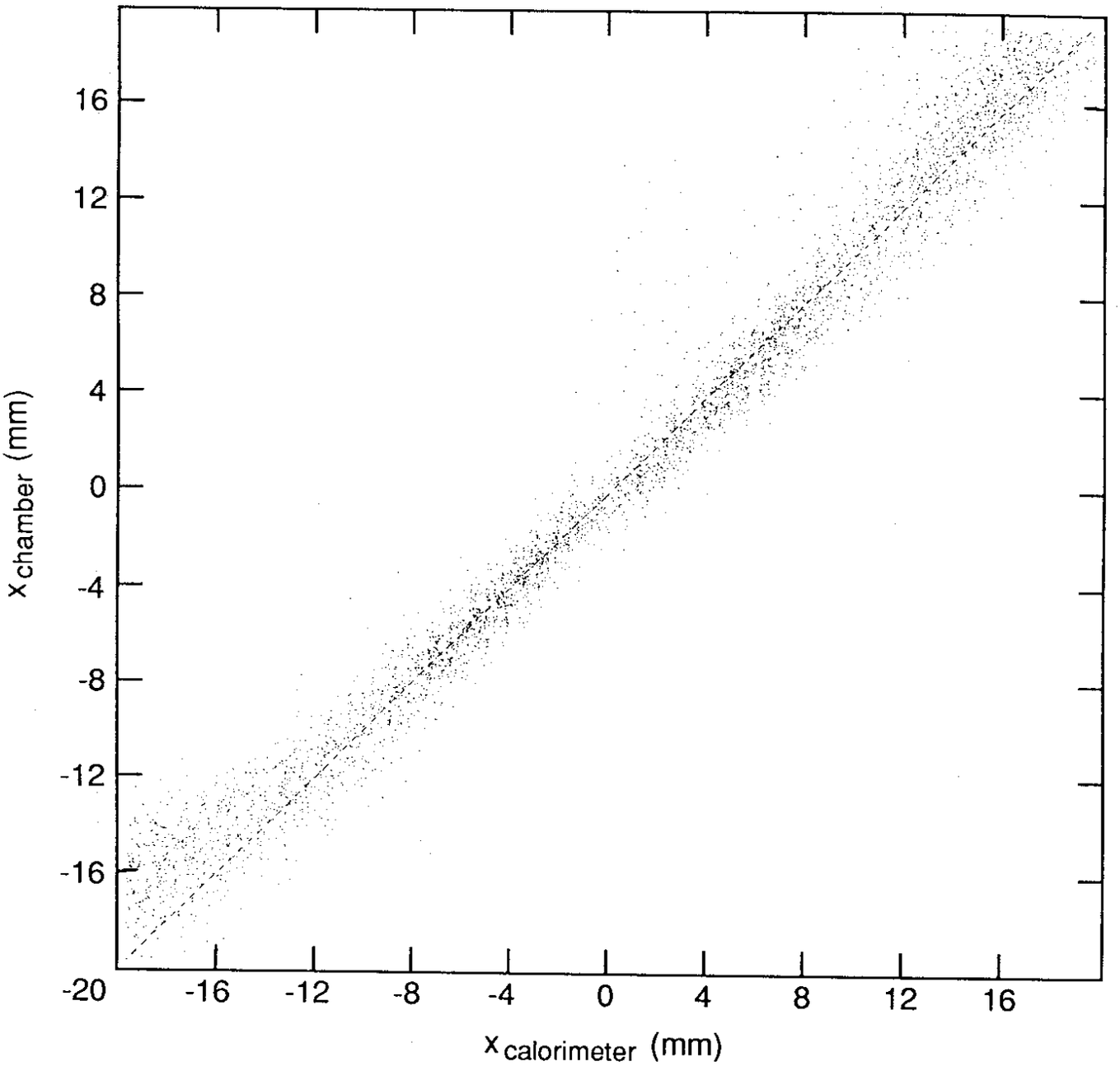
16
12
8
4
0
-4
-8
-12
-16
-20
-16
-12
-8
-4
0
4
8
12
16
x chamber (mm)
x calorimeter (mm)

Fig. 11 b)

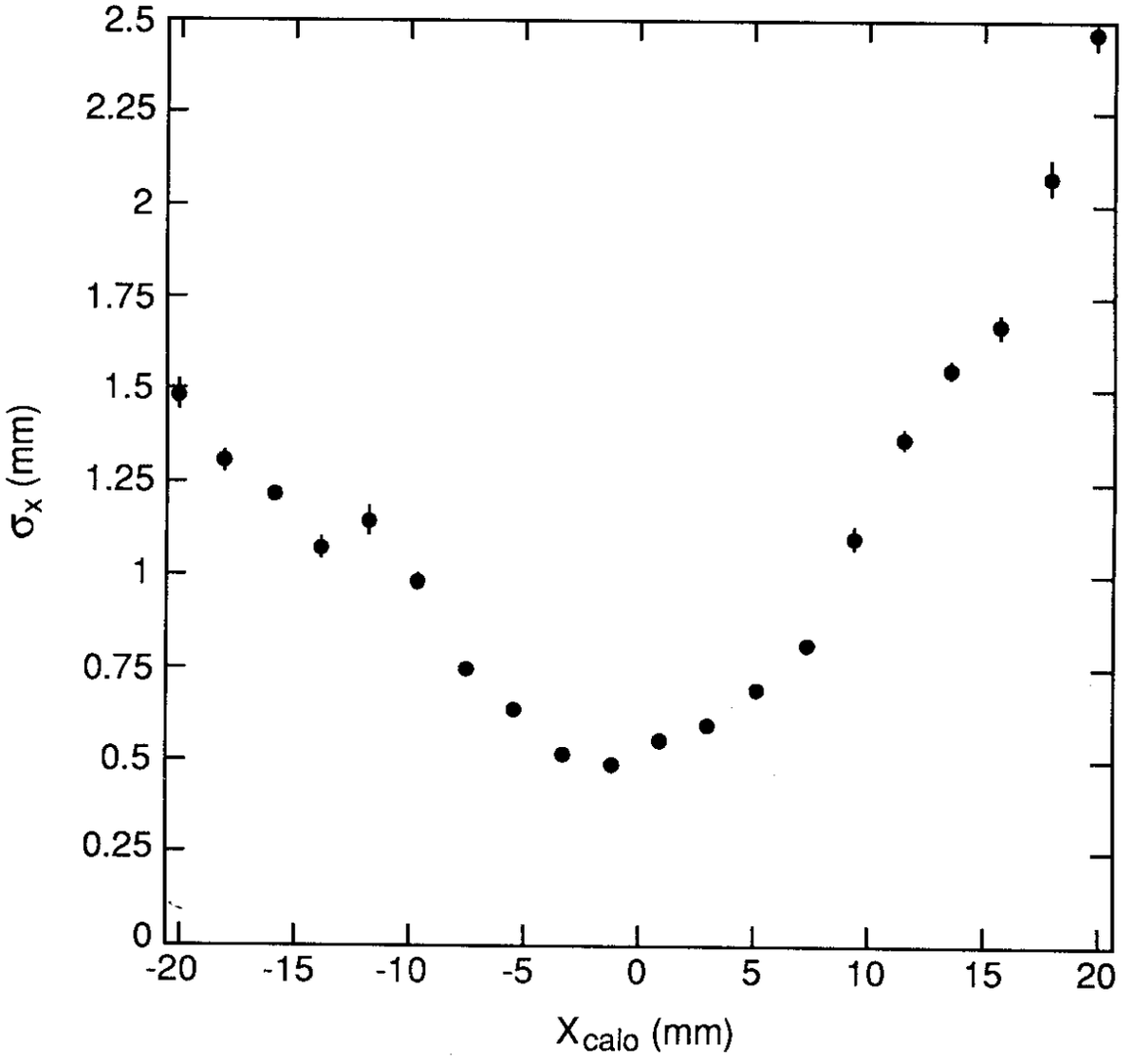
2.5
2.25
2
1.75
1.5
1.25
1
0.75
0.5
0.25
0
σ_x (mm)
-20
-15
-10
-5
0
5
10
15
20
X_{calo} (mm)

Fig. 12

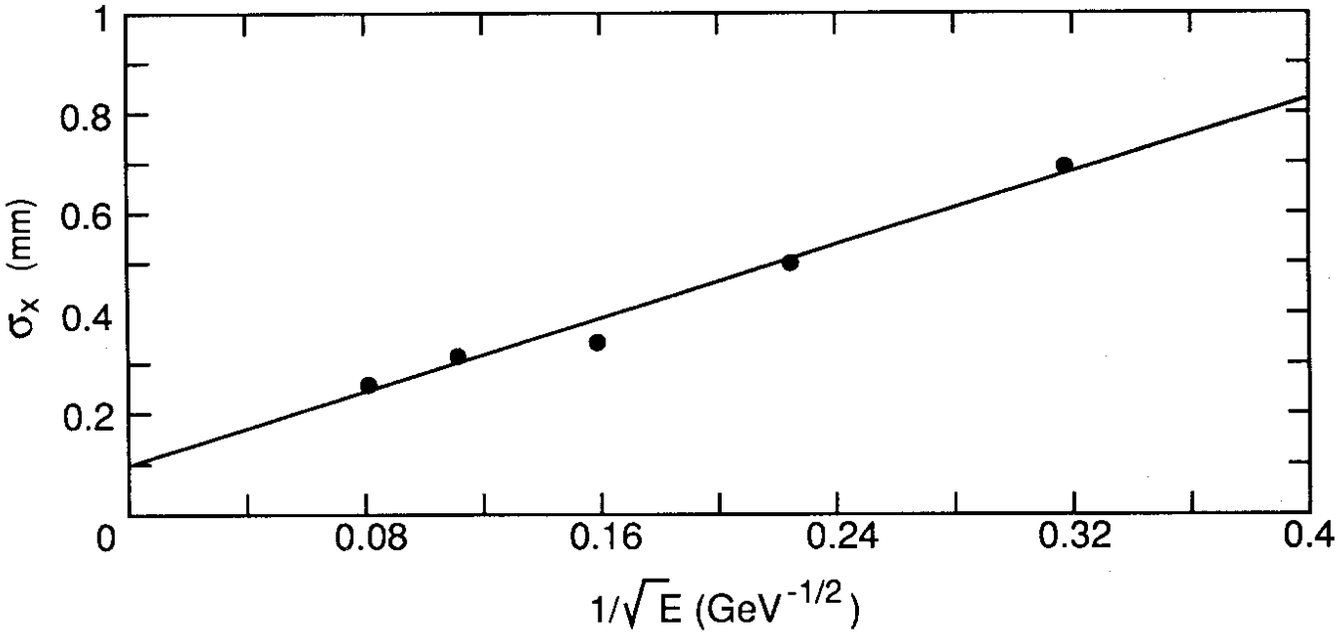

Fig. 13

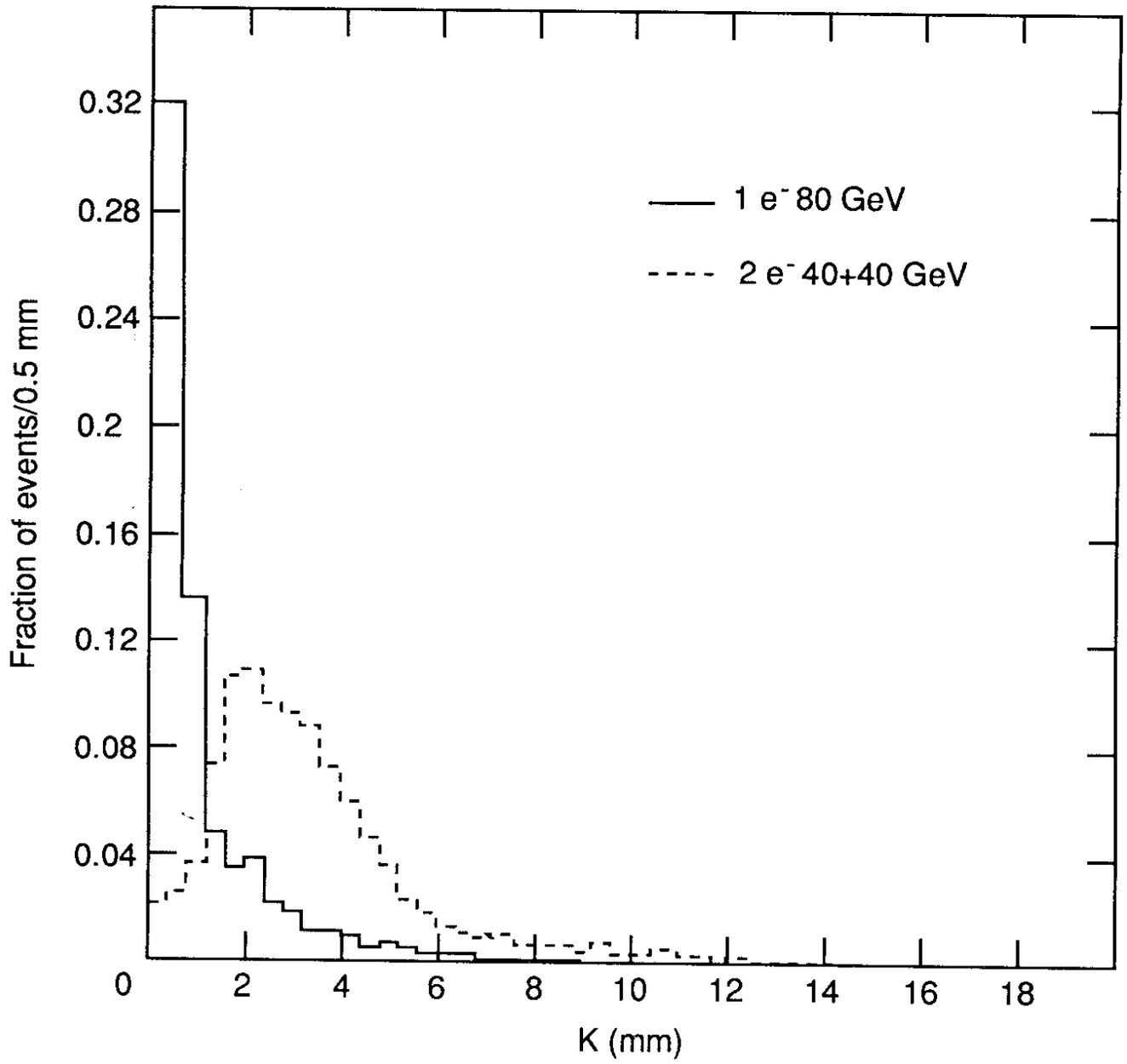
0.32
0.28
0.24
0.2
0.16
0.12
0.08
0.04
0
2
4
6
8
10
12
14
16
18
Fraction of events/0.5 mm
K (mm)
1 e⁻ 80 GeV
2 e⁻ 40+40 GeV

Fig. 14

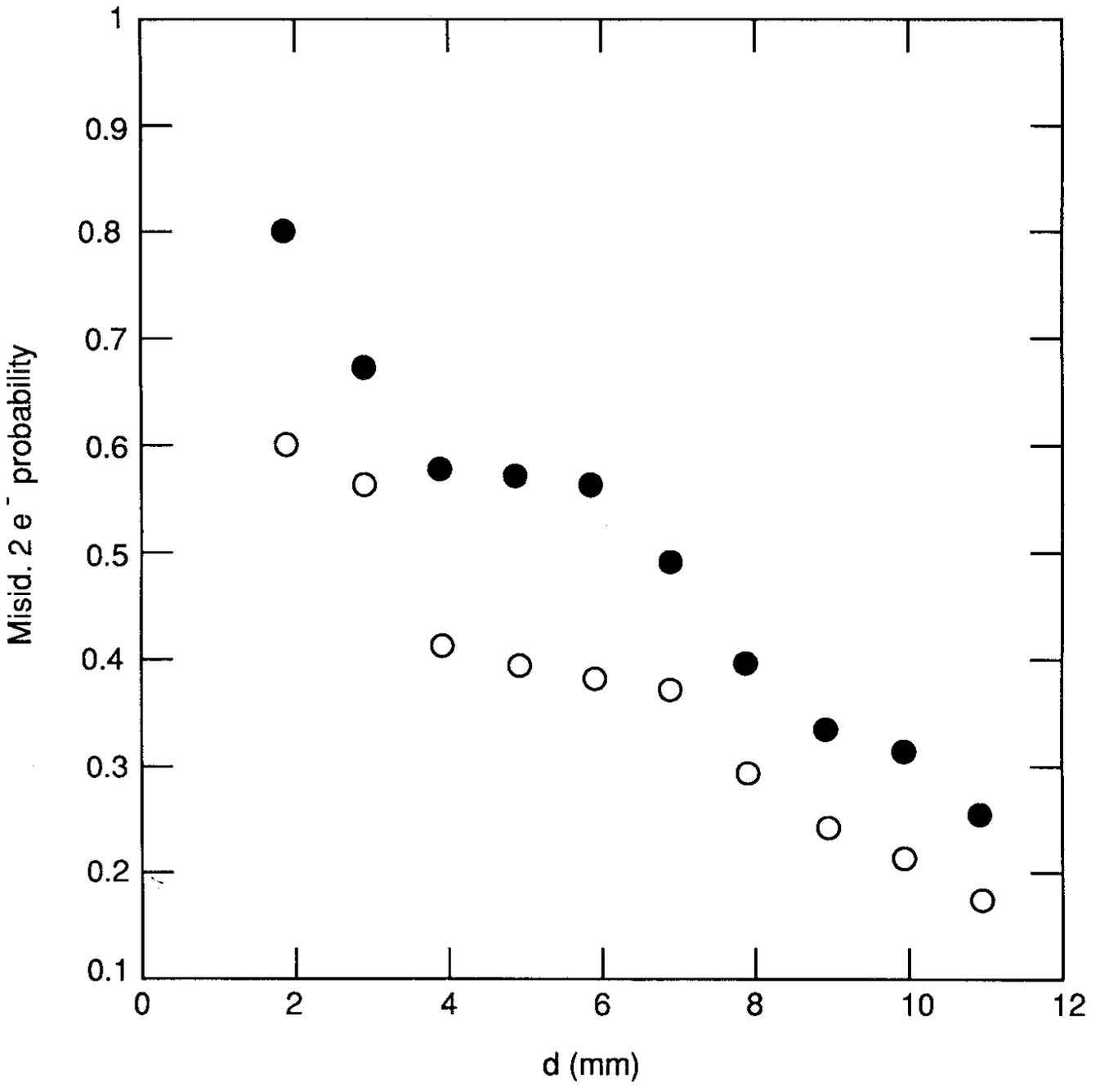

Fig. 15

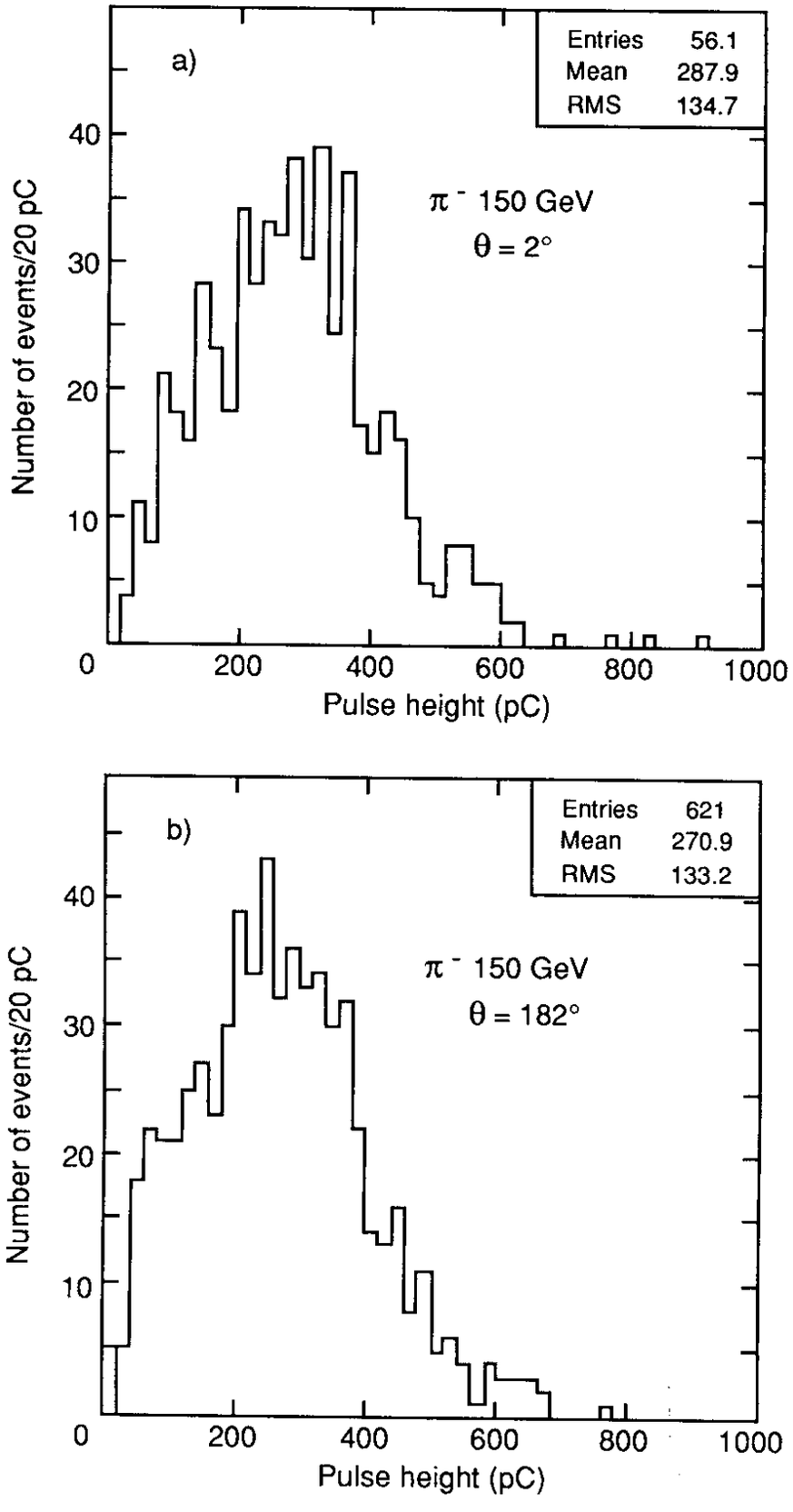
a)
Entries 56.1
Mean 287.9
RMS 134.7
π⁻ 150 GeV
θ = 2°
Number of events/20 pC
Pulse height (pC)
b)
Entries 621
Mean 270.9
RMS 133.2
π⁻ 150 GeV
θ = 182°
Number of events/20 pC
Pulse height (pC)

Fig. 16